Supplementary Material (ESI) for Dalton Transactions

Photocytotoxicity and DNA cleavage activity of L-arg and L-lys Schiff base oxovanadium(IV) complexes having phenanthroline bases†

Pijus K. Sasmal,[a] Ritankar Majumdar,[b] Rajan R. Dighe [b] and Akhil R. Chakravarty*[a]

[a] *Department of Inorganic and Physical Chemistry, Indian Institute of Science, Bangalore 560012, India. Fax: (+91)80-23600683; Tel: +91-80-22932533; E-mail: arc@ipc.iisc.ernet.in*

[b] *Department of Molecular Reproduction, Development and Genetics, Indian Institute of Science, Bangalore 560012, India.*

Electronic Supplementary Information

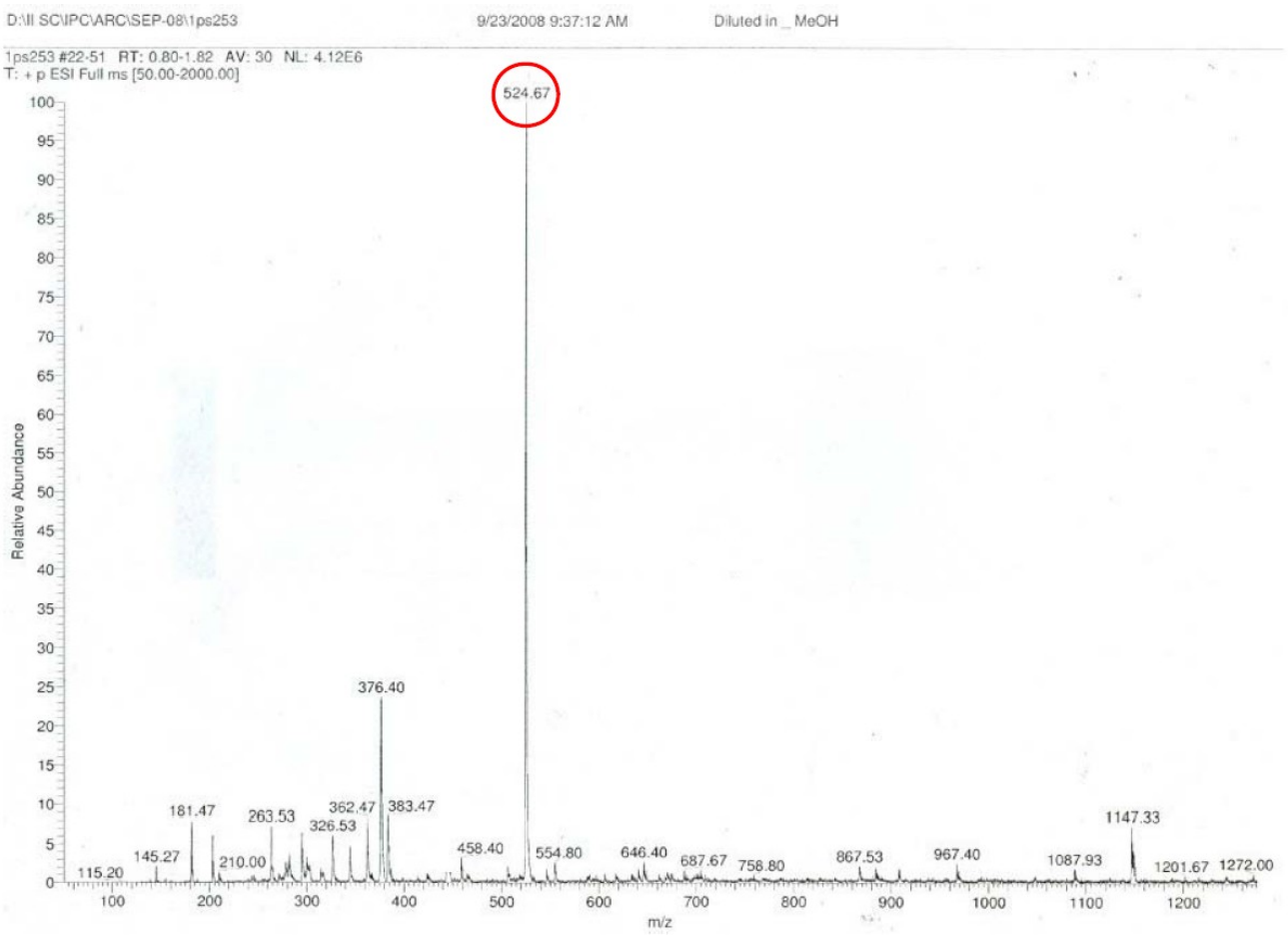

ESI Fig. S1. The ESI-MS spectrum of [VO(sal-argH)(phen)]Cl (**1**) in MeOH showing the peak at 524.67 (m/z) assignable to $[M]^+$. The 376.40 (m/z) peak corresponds to $[VO(sal\text{-}argH)(MeOH)]^+$ generated from the complex.

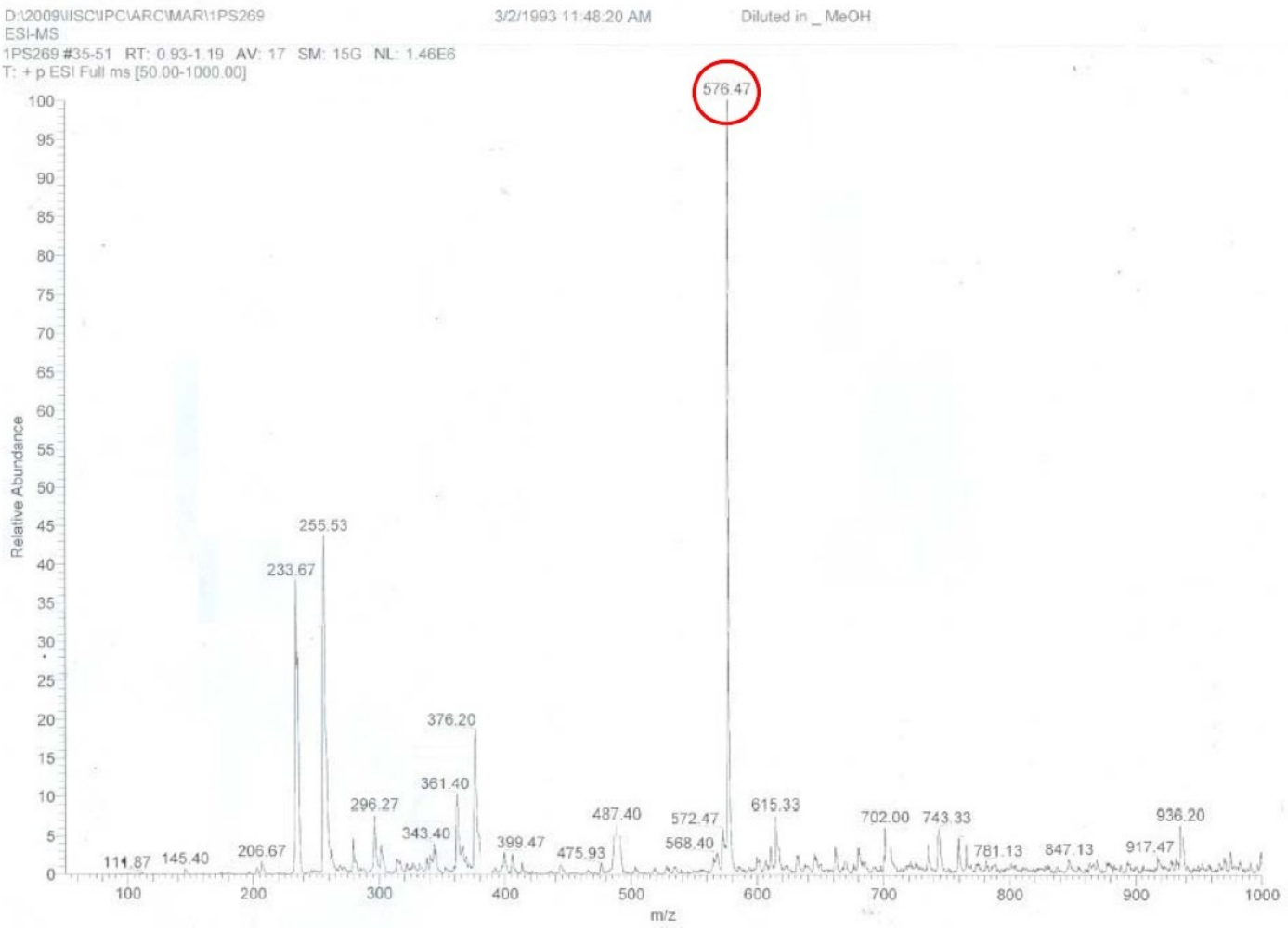

ESI Fig. S2. The ESI-MS spectrum of [VO(sal-argH)(dpq)]Cl (**2**) in MeOH showing the peak at 576.47 (m/z) assignable to $[M]^+$. The 376.20 (m/z), 255.53 (m/z) and 233.67 (m/z) peaks correspond to $[VO(sal\text{-}argH)(MeOH)]^+$, $[dpq + Na]^+$ and $[dpq+H]^+$, respectively, generated from the complex.

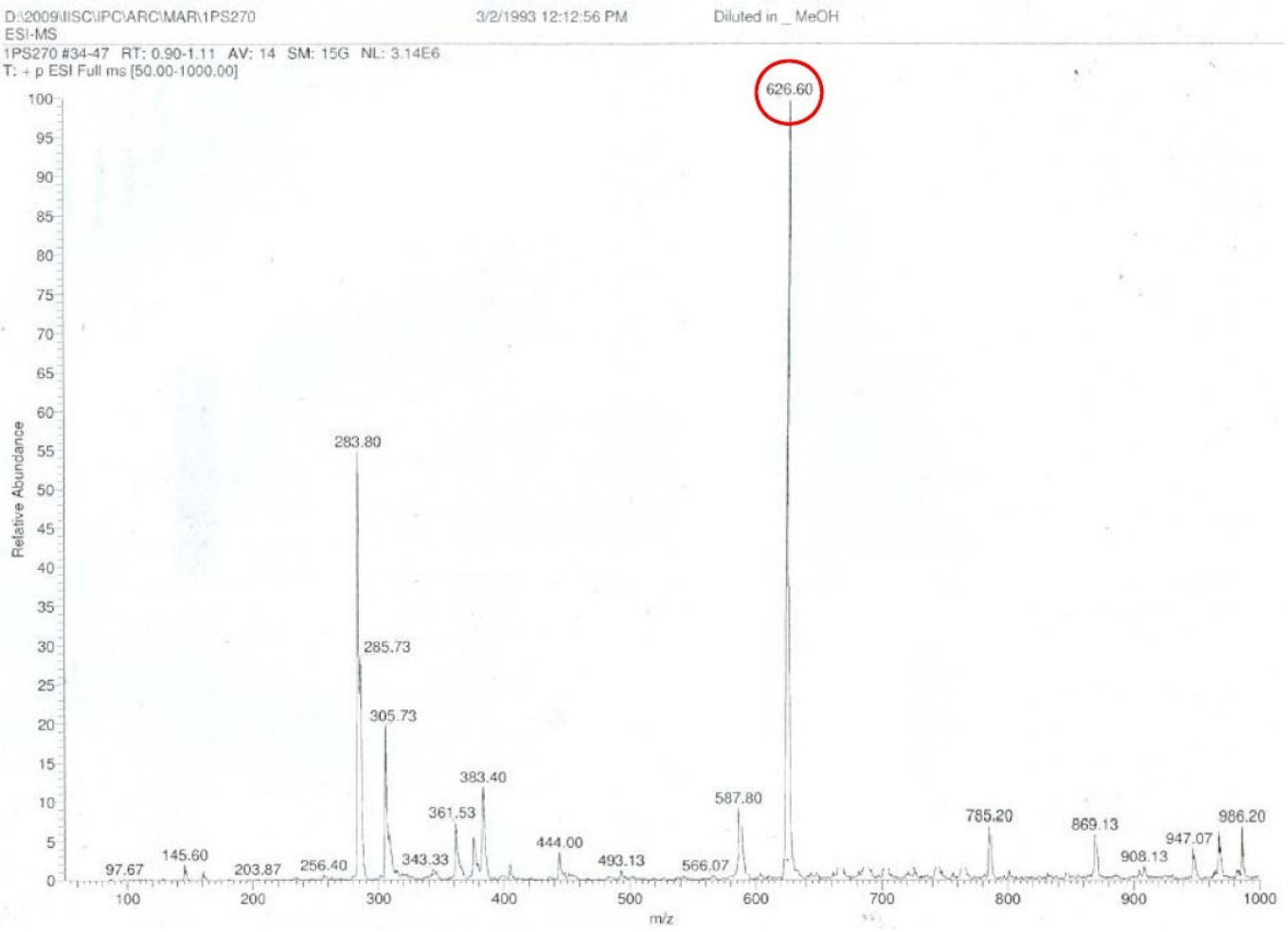

ESI Fig. S3. The ESI-MS spectrum of [VO(sal-argH)(dppz)]Cl (**3**) in MeOH showing the peak at 626.60 (m/z) assignable to $[M]^+$. The 305.73 (m/z) and 283.80 (m/z) peaks correspond to $[dppz+Na]^+$ and $[dppz+H]^+$, respectively, generated from the complex.

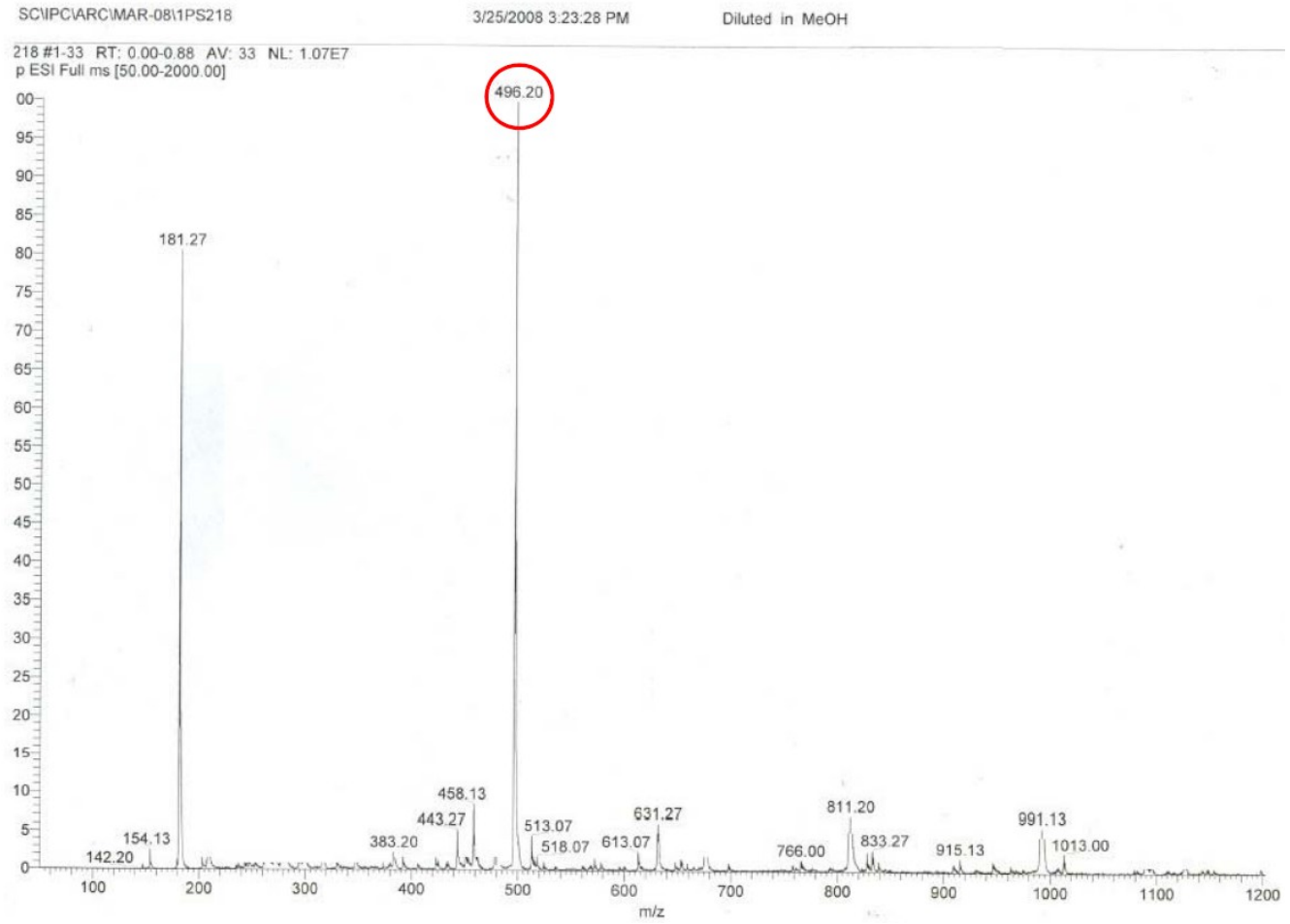

ESI Fig. S4. The ESI-MS spectrum of [VO(sal-lysH)(phen)]Cl (**4**) in MeOH showing the peak at 496.20 (m/z) assignable to $[M]^+$. The peak at 181.27 (m/z) corresponds to $[phen+H]^+$ species generated from the complex.

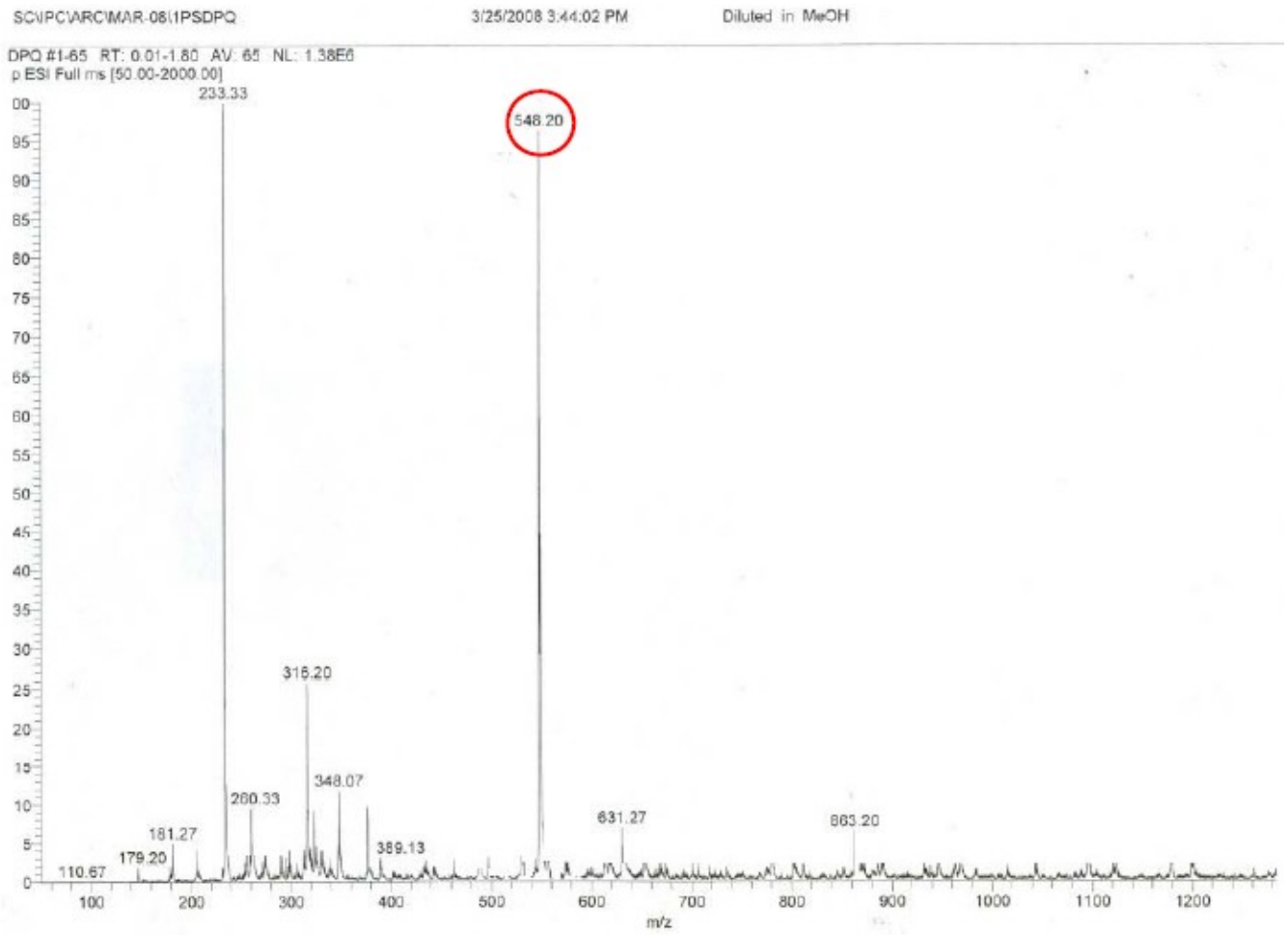

ESI Fig. S5. The ESI-MS spectrum of [VO(sal-lysH)(dpq)]Cl (**5**) in MeOH showing the peak at 548.20 (m/z) assignable to $[M]^+$. The 316.20 (m/z) and 233.33 (m/z) peaks correspond to $[VO(sal\text{-}lysH)]^+$ and $[dpq+H]^+$, respectively, generated from the complex.

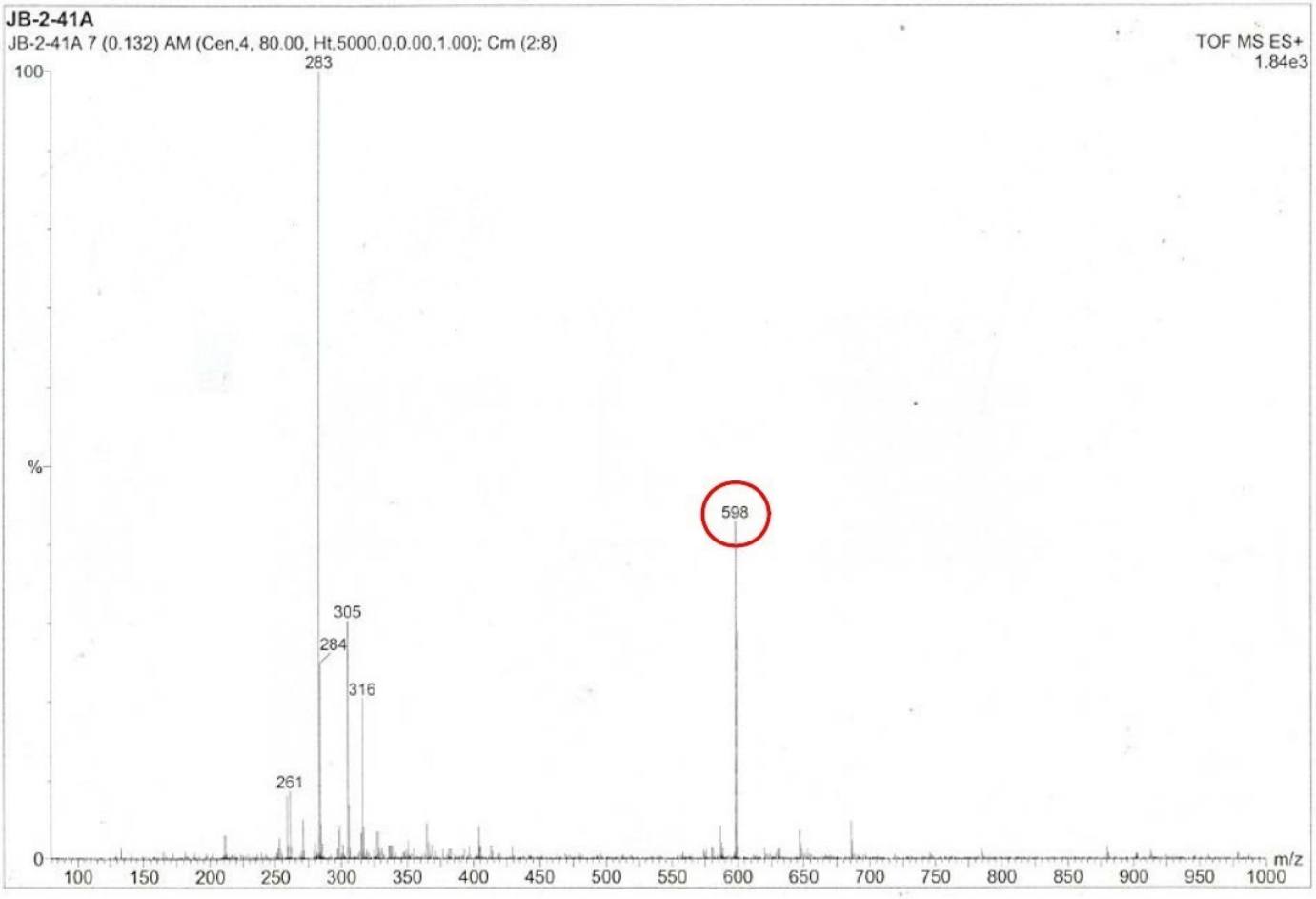

ESI Fig. S6. The ESI-MS spectrum of [VO(sal-lysH)(dppz)]Cl (**6**) in MeOH showing the peak at 598 (m/z) assignable to $[M]^+$. The 316 (m/z), 305 (m/z) and 283 (m/z) peaks correspond to $[VO(sal\text{-}lysH)]^+$, $[dppz+Na]^+$ and $[dppz+H]^+$, respectively, generated from the complex.

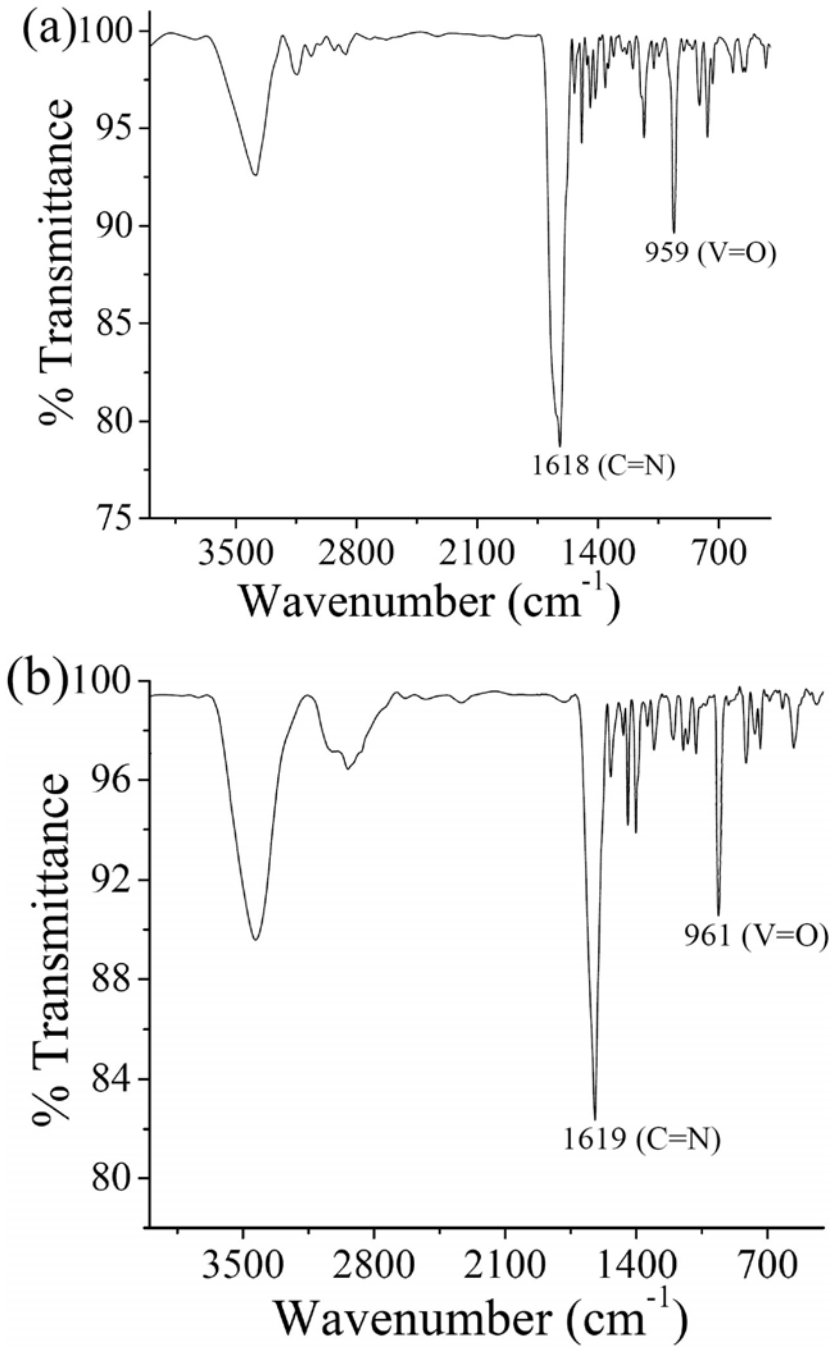

ESI Fig. S7. IR spectra of (a) [VO(sal-argH)(dppz)]Cl (**3**) and (b) [VO(sal-lysH)(dpq)]Cl (**5**) in KBr phase showing their characteristic peaks of C=N and V=O.

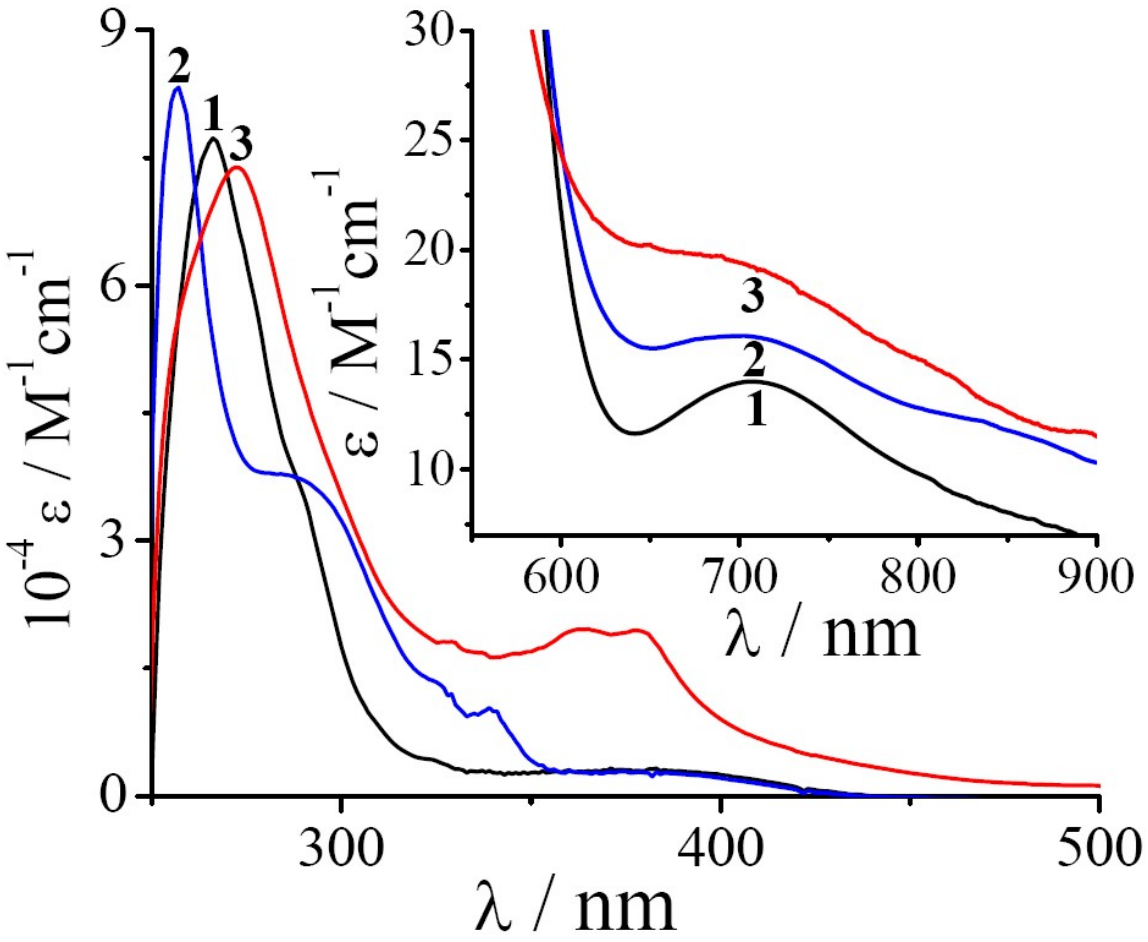

ESI Fig. S8. Electronic spectra of the complexes [VO(sal-argH)(phen)]Cl (**1**, —), [VO(sal-argH)(dpq)]Cl (**2**, —) and [VO(sal-argH)(dppz)]Cl (**3**, —) in 20% DMF-Tris-HCl buffer with the inset showing the d-d bands in the visible region.

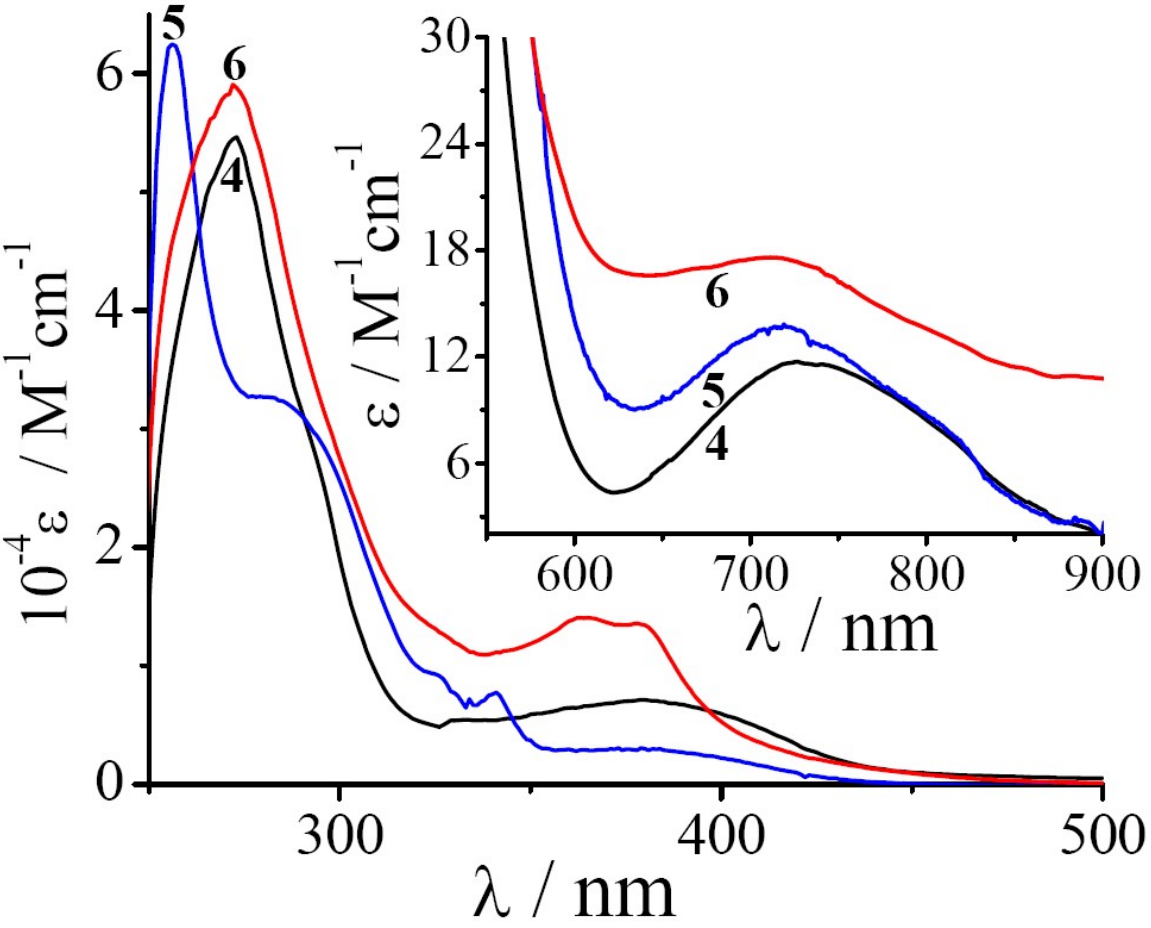

ESI Fig. S9. Electronic spectra of the complexes [VO(sal-lysH)(phen)]Cl (**4**, —), [VO(sal-lysH)(dpq)]Cl (**5**, —) and [VO(sal-lysH)(dppz)]Cl (**6**, —) in 20% DMF-Tris-HCl buffer with the inset showing the d-d bands in the visible region.

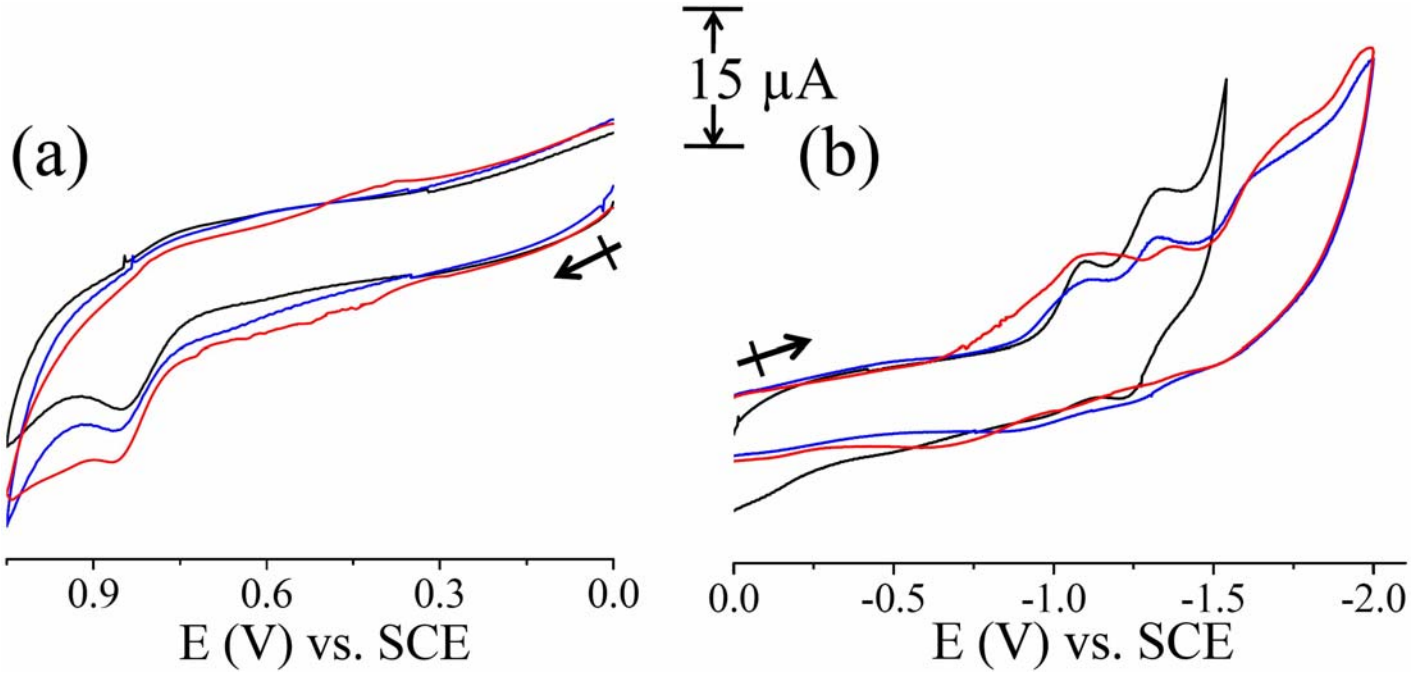

ESI Fig. S10. Cyclic voltammograms of the complexes [VO(sal-argH)(B)]Cl [B = phen, **1** (—); dpq, **2** (—); and dppz, **3** (—)] showing (a) anodic scans and (b) cathodic scans in 25% DMF-Tris-HCl buffer at a scan speed of 50 mV s^{-1} and 0.1 M KCl as a supporting electrolyte.

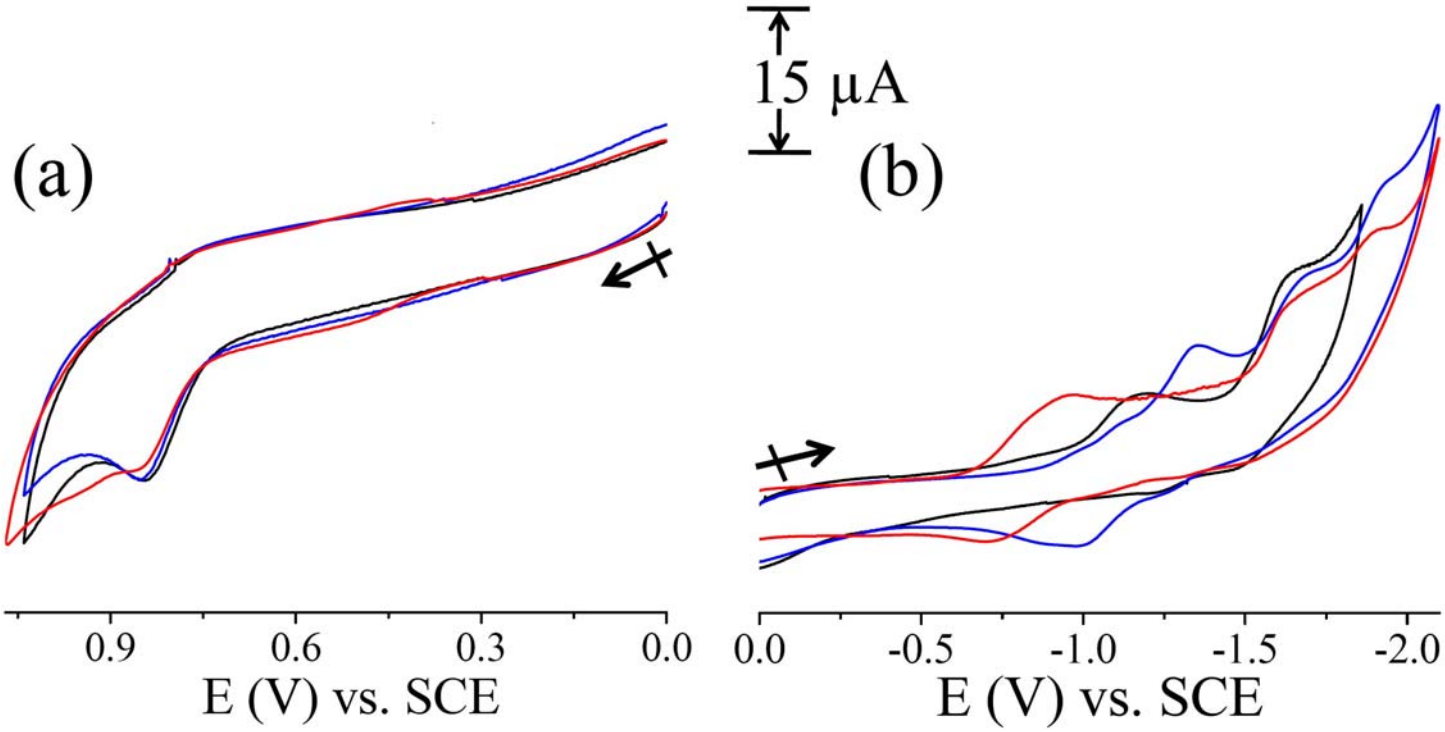

ESI Fig. S11. Cyclic voltammograms of the complexes [VO(sal-lysH)(B)]Cl [B = phen, **4** (—); dpq, **5** (—); and dppz, **6** (—)] showing (a) anodic scans and (b) cathodic scans in 25% DMF-Tris-HCl buffer at a scan speed of 50 mV s^{-1} and 0.1 M KCl as a supporting electrolyte.

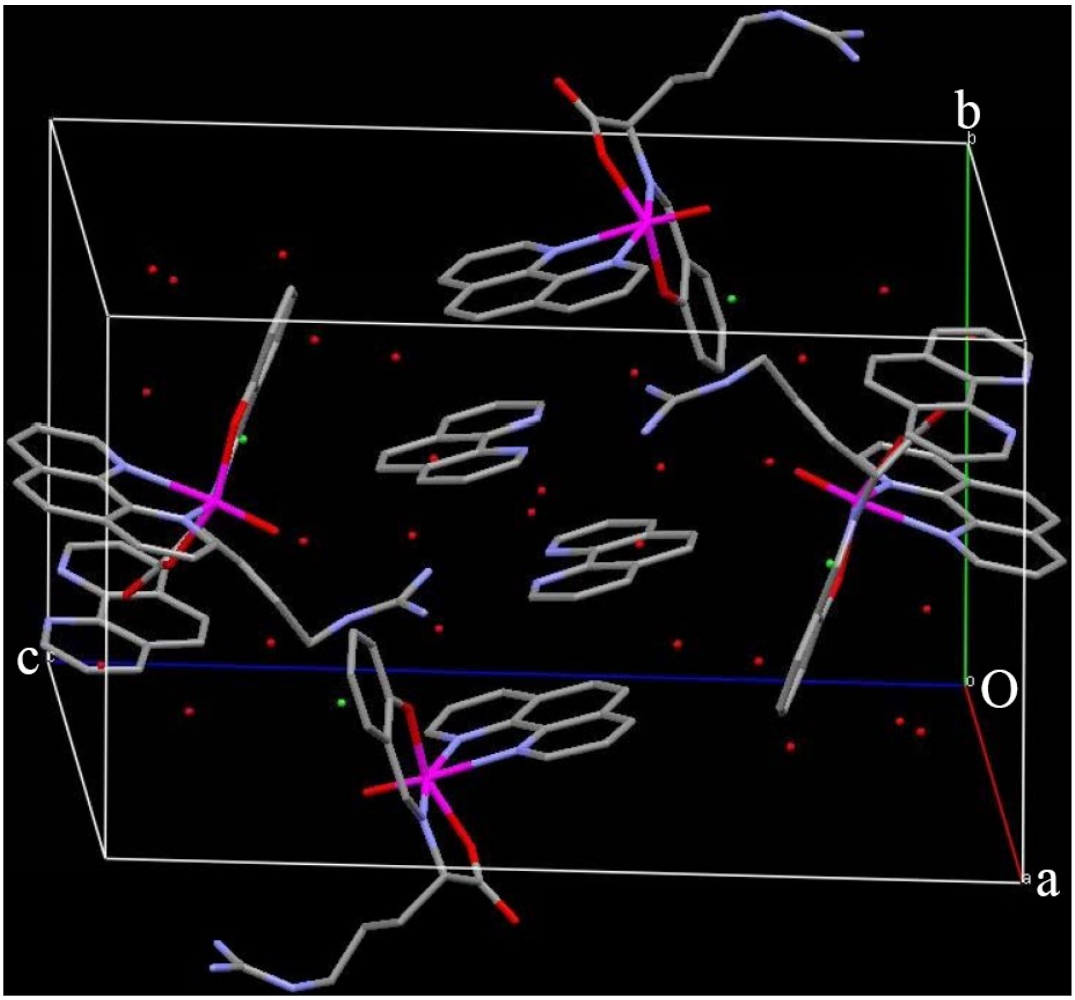

ESI Fig. S12. Unit cell packing diagram of [VO(sal-argH)(phen)]Cl·phen·7H_2O (**1**· phen·7H_2O).

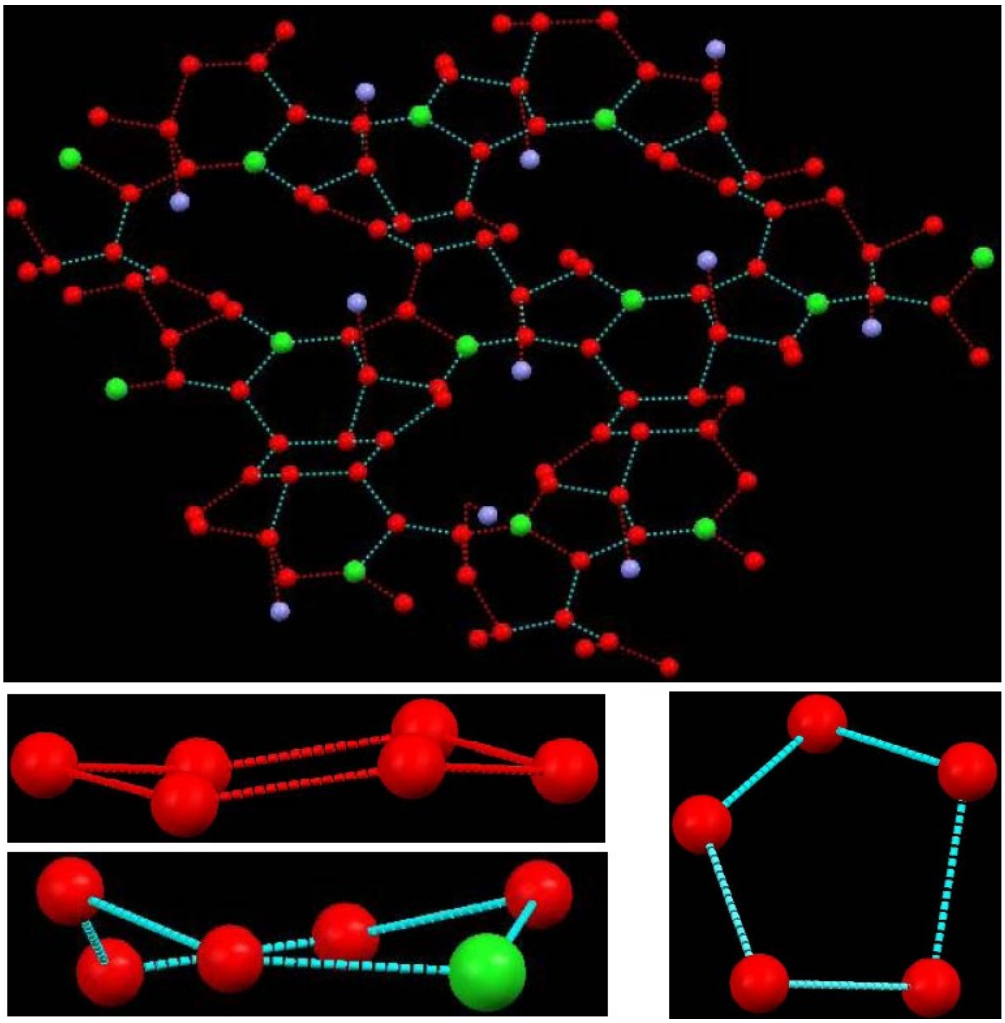

ESI Fig. S13. Crystal structure of [VO(sal-argH)(phen)]Cl·phen·7H_2O (**1**· phen·7H_2O) showing the hydrogen bonding network formed by the water molecules and the chloride ion with five- and six-membered rings. The six-membered ring formed by only water molecules shows chair conformation. Color codes: red, oxygen atom; green, chloride ion; blue, nitrogen atom.

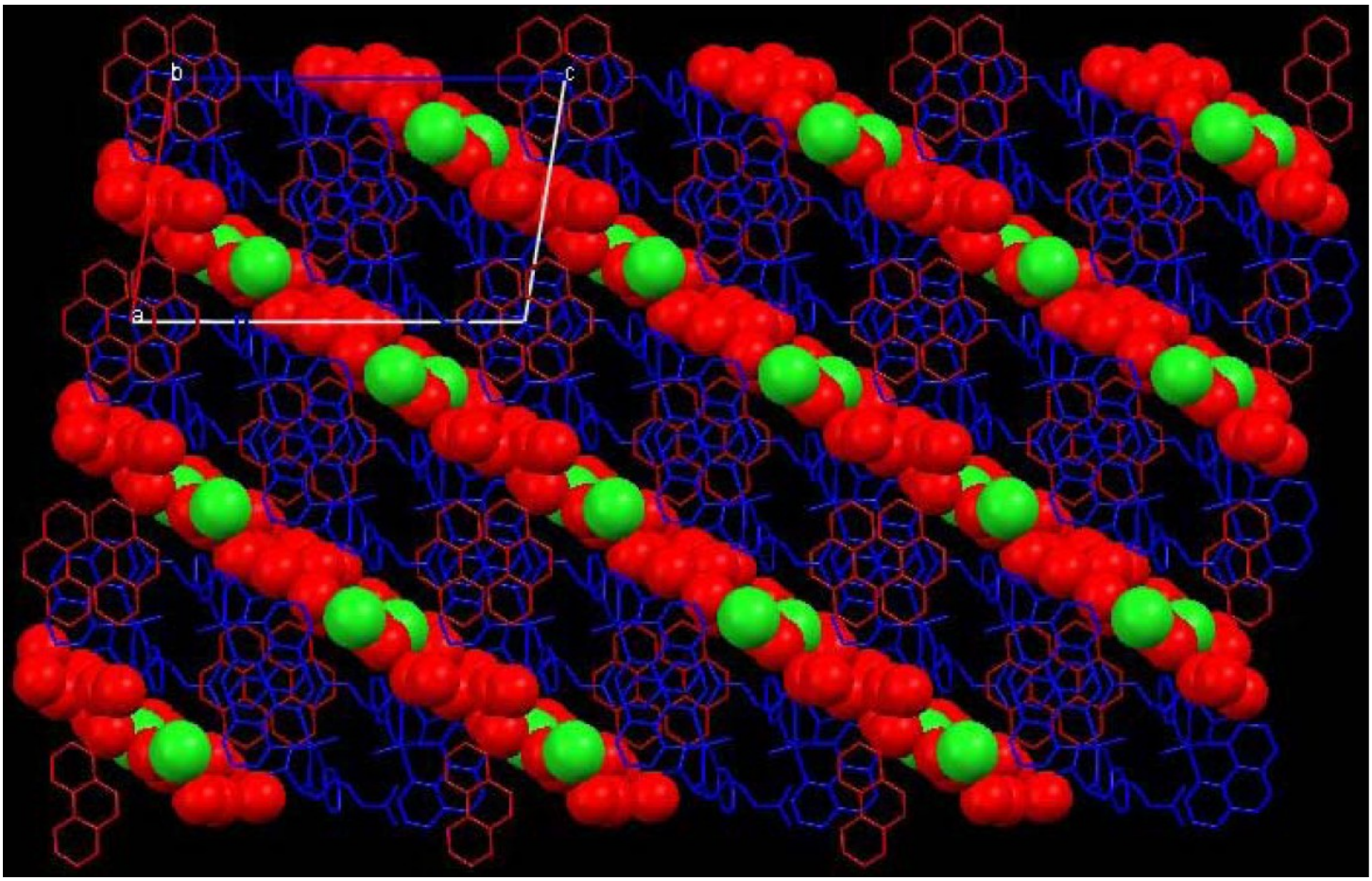

ESI Fig. S14. Crystal structure of [VO(sal-argH)(phen)]Cl·phen·7H_2O (**1**· phen·7H_2O) showing the complex back bone and the water channel in the lattice. The red and green ball-shaped models are water and chloride atom, respectively.

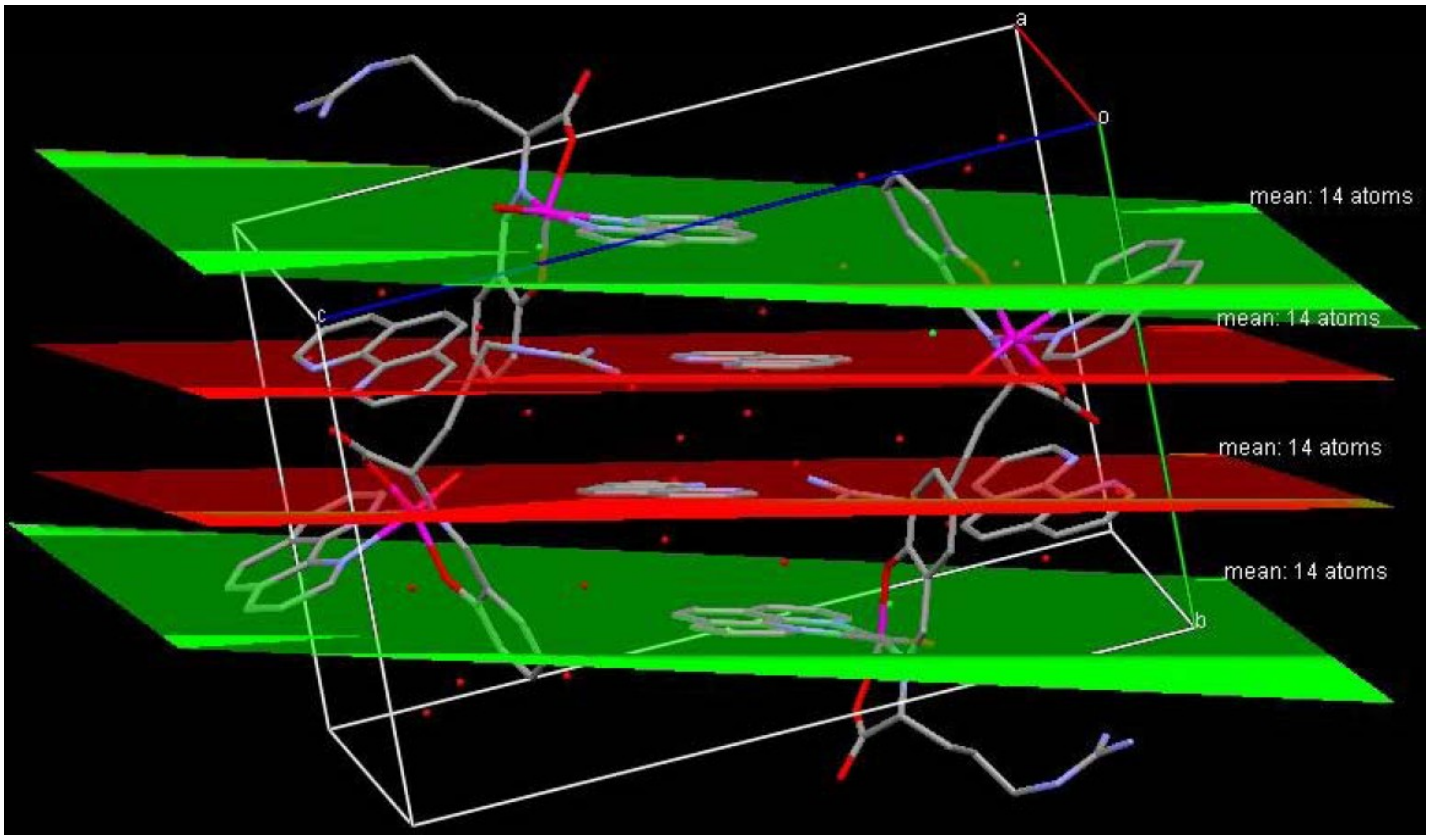

ESI Fig. S15. Crystal structure of [VO(sal-argH)(phen)]Cl·phen·7H_2O (**1**· phen·7H_2O) showing coplanar orientation of two free phenanthroline bases in the unit cell (red planes) and the orientation of the nearest phen bases bound to the metal center (green planes).

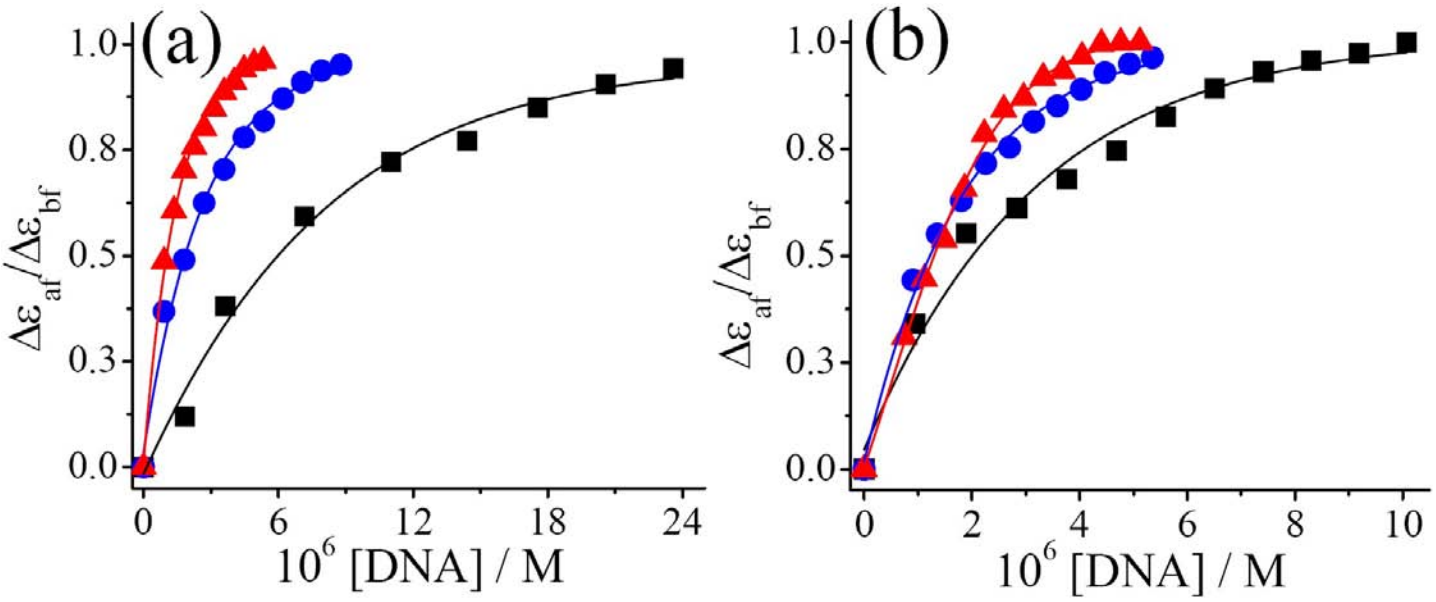

ESI Fig. S16. (a) The plot of least-squares fit of $\Delta\varepsilon_{af}/\Delta\varepsilon_{bf}$ vs. [CT DNA] for the complexes [VO(sal-argH)(phen)]Cl (**1**, ■), [VO(sal-argH)(dpq)]Cl (**2**, ●) and [VO(sal-argH)(dppz)]Cl (**3**, ▲). (b) The plot of least-squares fit of $\Delta\varepsilon_{af}/\Delta\varepsilon_{bf}$ vs. [DNA] for [VO(sal-lysH)(dppz)]Cl (**6**) with poly(dG)·poly(dC) (■), **6** with CT DNA (●) and **6** with poly(dA)·poly(dT) (▲).

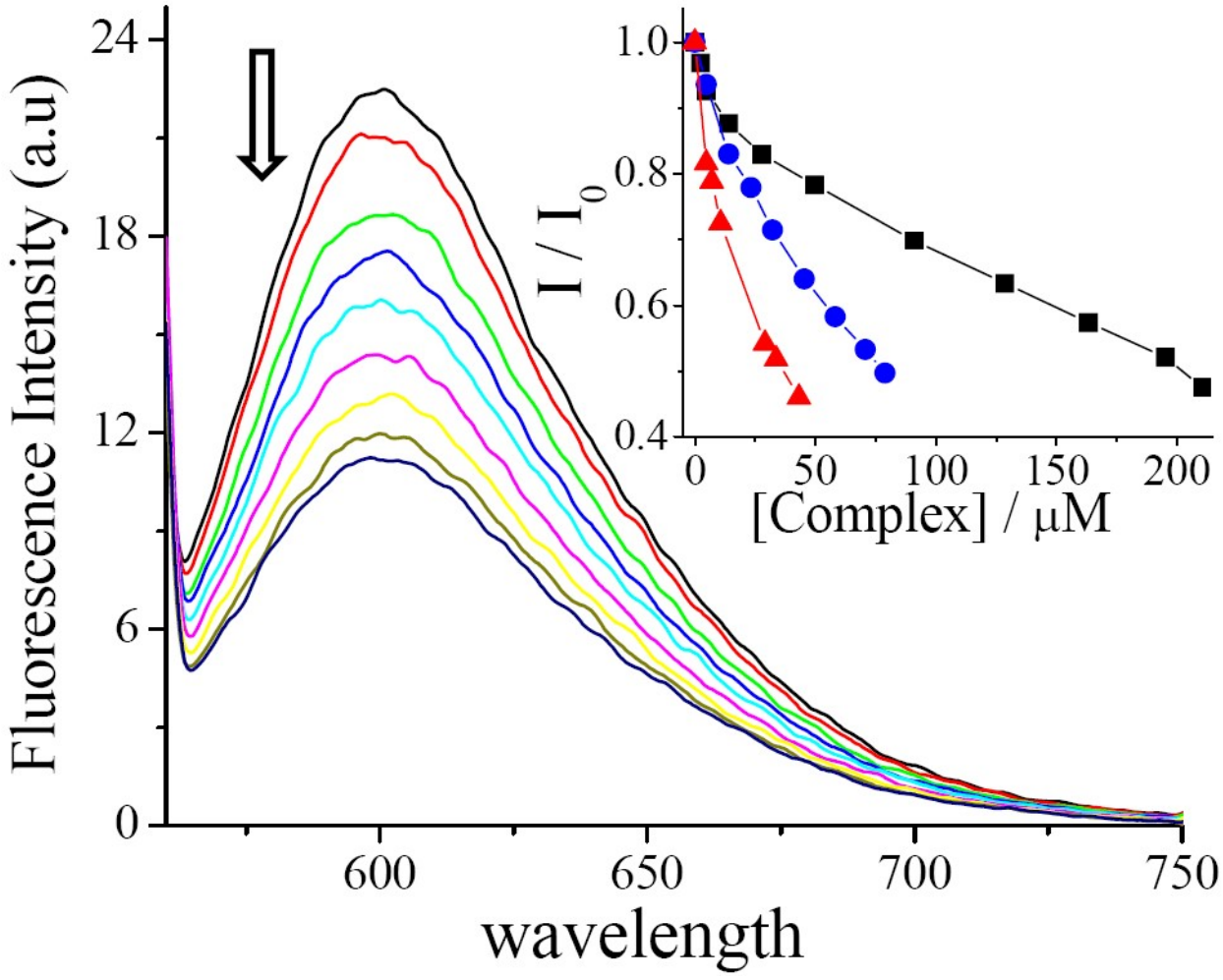

ESI Fig. S17. Emission spectral traces of [VO(sal-argH)(dpq)]Cl (**2**) using 325 μM calf thymus DNA-bound ethidium bromide (1.3 μM) at different complex concentrations in 5 mM Tris-HCl buffer (pH, 7.2) at 25 ºC. The inset shows the plots for the complexes [VO(sal-argH)(phen)]Cl (**1**, ■), **2** (●) and [VO(sal-argH)(dppz)]Cl (**3**, ▲).

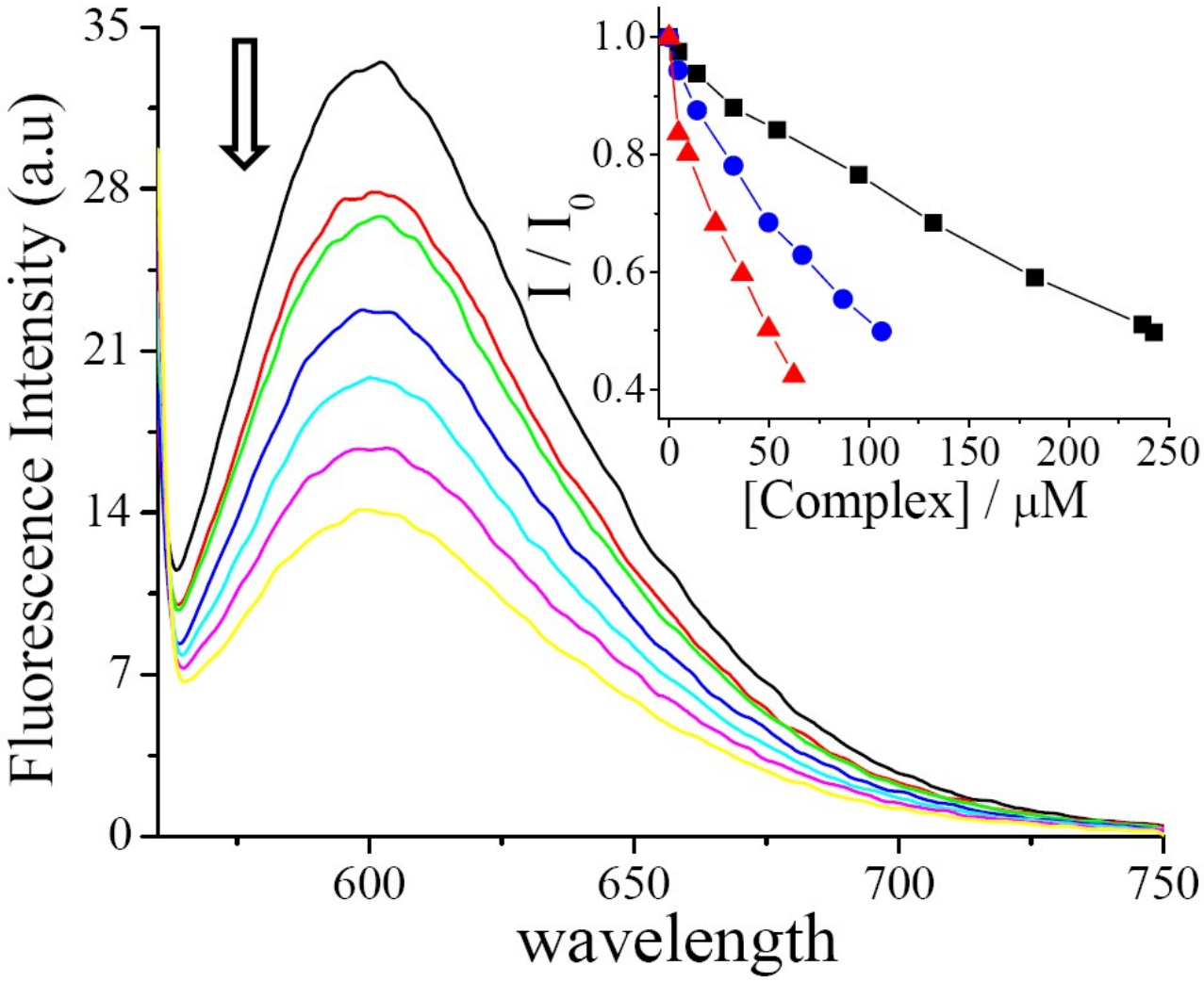

ESI Fig. S18. Emission spectral traces of [VO(sal-lysH)(dppz)]Cl (**6)** using 325 μM calf thymus DNA-bound ethidium bromide (1.3 μM) at different complex concentrations in 5 mM Tris-HCl buffer (pH, 7.2) at 25 ºC. The inset shows the plots for the complexes [VO(sal-lysH)(phen)]Cl (**4**, ■), [VO(sal-lysH)(dpq)]Cl (**5**, ●) and **6** (▲).

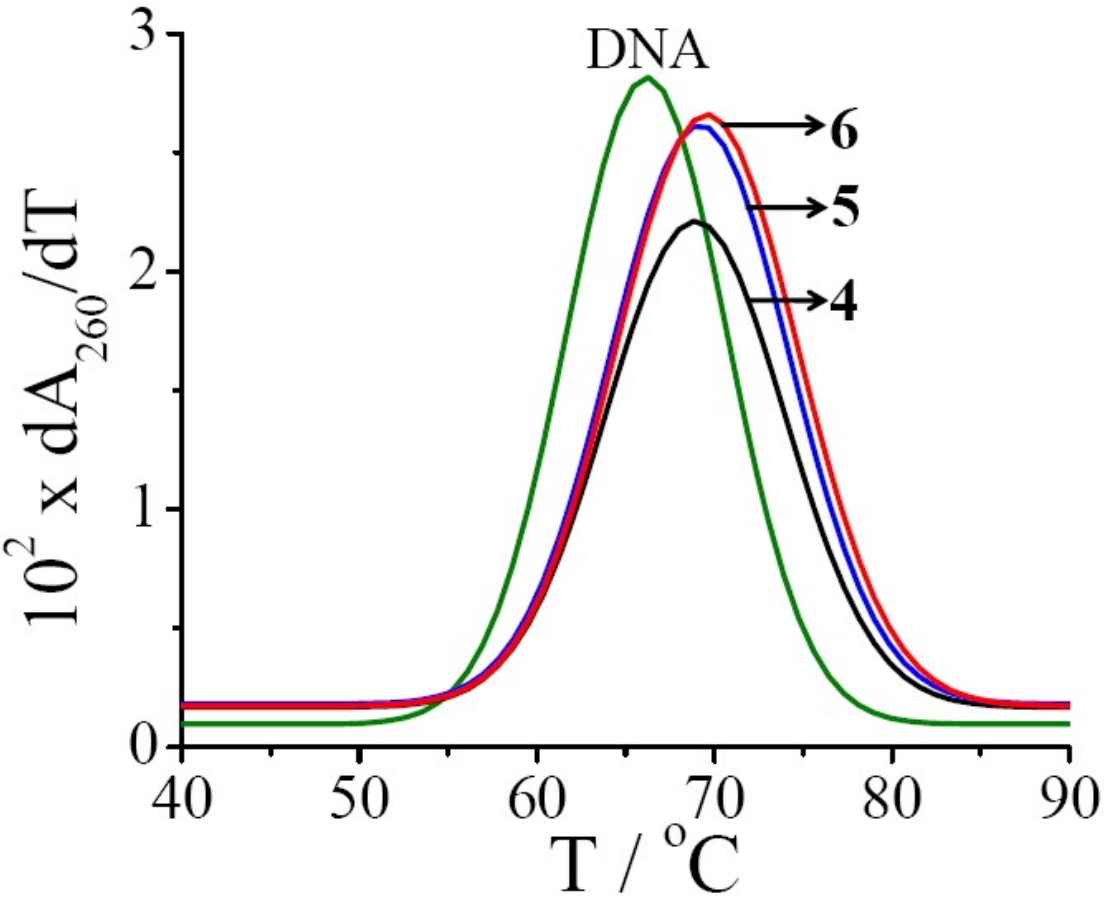

ESI Fig. S19. Thermal denaturation plots of 170 μM CT DNA alone and in the presence of the complexes [VO(sal-lysH)(B)]Cl (B: phen, **4**; dpq, **5**; dppz, **6**) (10 μM) in 5 mM phosphate buffer (pH, 6.85).

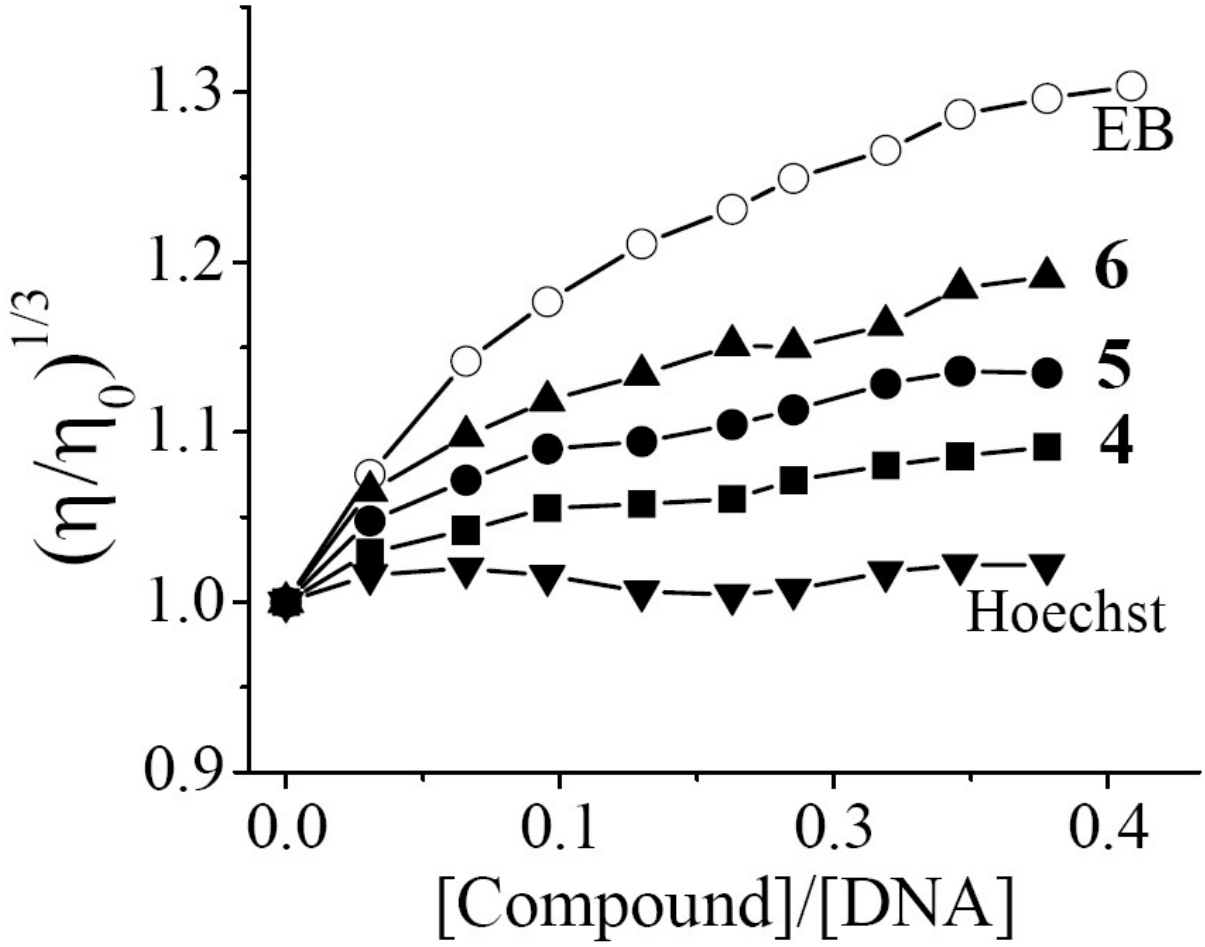

ESI Fig. S20. The effect of increasing concentration of the compounds [VO(sal-lysH)(B)]Cl [B: phen, **4** (■); dpq, **5** (●); dppz, **6** (▲)], ethidium bromide (EB, o) and Hoechst-33258 (▼) on the relative viscosities of CT-DNA at 37.0 (±0.1) °C in 5 mM Tris-HCl buffer (pH 7.2, [DNA] = 140 μM). EB and Hoechst 33258 used as control species are DNA intercalating and groove binding species, respectively.

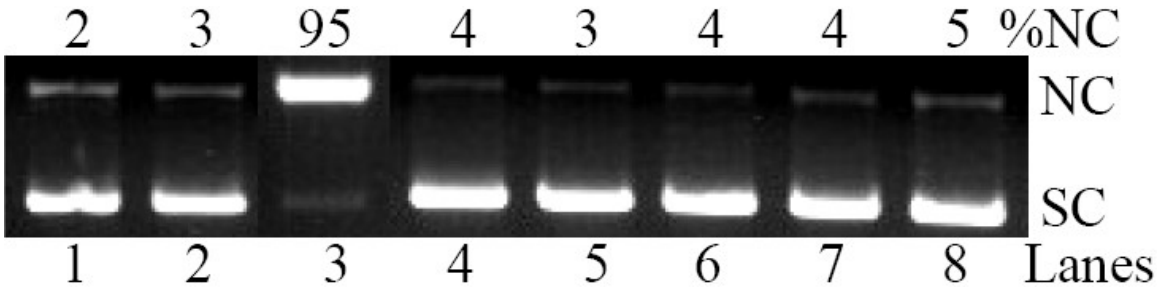

ESI Fig. S21. Cleavage of SC pUC19 DNA (0.2 μg, 30 μM) by [VO(sal-argH)(dpq)]Cl (**2**) and [VO(sal-lysH)(dppz)]Cl (**6**) (80 μM) in the presence of reducing agent MPA (0.5 mM) and oxidizing agent H_2O_2 (0.5 mM) in 50 mM Tris-HCl/NaCl buffer (pH 7.2) containing 1.5% DMF under dark reaction condition. The reaction conditions are given below in a tabular form. The copper-phen species is used as a control that cleaves DNA at only 5 μM complex concentration in the presence of MPA, while the oxovanadium(IV) complexes do not any chemical nuclease activity even at a high complex concentration of 80 μM.

Lane No	Reaction conditions
1	DNA control
2	DNA + MPA
3	DNA + $[Cu(phen)_2(H_2O)](ClO_4)_2$ (5 μM) + MPA
4	DNA + **2** + MPA
5	DNA + **6** + MPA
6	DNA + H_2O_2
7	DNA + **2** + H_2O_2
8	DNA + **6** + H_2O_2

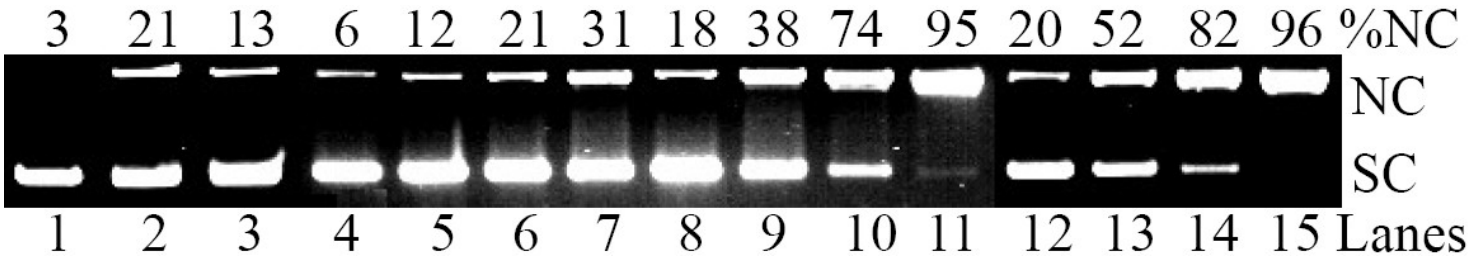

ESI Fig. S22. Cleavage of SC pUC19 DNA (0.2 μg, 30 μM) by the complexes [VO(sal-argH)(B)]Cl (B: phen, **1**; dpq, **2**; dppz, **3**; 15 μM) in 50 mM Tris-HCl/NaCl buffer (pH, 7.2) containing 1.5% DMF on photo-irradiation at 365 nm (6 W) at different exposure times. Detailed reaction conditions are given below in a tabular form.

Lane No	Reaction conditions
1	DNA control (1.0 h)
2	DNA + dppz (15 μM) (2.0 h)
3	DNA + sal-argH_2 (15 μM) (2.0 h)
4-7	DNA + complex **1** (0.5, 1.0, 1.5, 2.0 h)
8-11	DNA + complex **2** (0.5, 1.0, 1.5, 2.0 h)
12-15	DNA + complex **3** (0.5, 1.0, 1.5, 2.0 h)

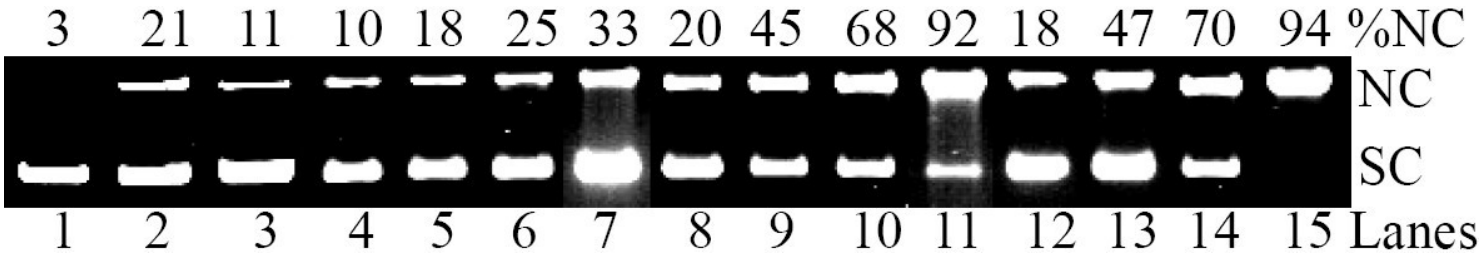

ESI Fig. S23. Cleavage of SC pUC19 DNA (0.2 μg, 30 μM) by the complexes [VO(sal-lysH)(B)]Cl (B: phen, **4**; dpq, **5**; dppz, **6**; 15 μM) in 50 mM Tris-HCl/NaCl buffer (pH, 7.2) containing 1.5% DMF on photo-irradiation at 365 nm (6 W) at different exposure times. Detailed reaction conditions are given below in a tabular form.

Lane No	Reaction conditions
1	DNA control (1.0 h)
2	DNA + dppz (15 μM) (2.0 h)
3	DNA + sal-argH_2 (15 μM) (2.0 h)
4-7	DNA + complex **4** (0.5, 1.0, 1.5, 2.0 h)
8-11	DNA + complex **5** (0.5, 1.0, 1.5, 2.0 h)
12-15	DNA + complex **6** (0.5, 1.0, 1.5, 2.0 h)

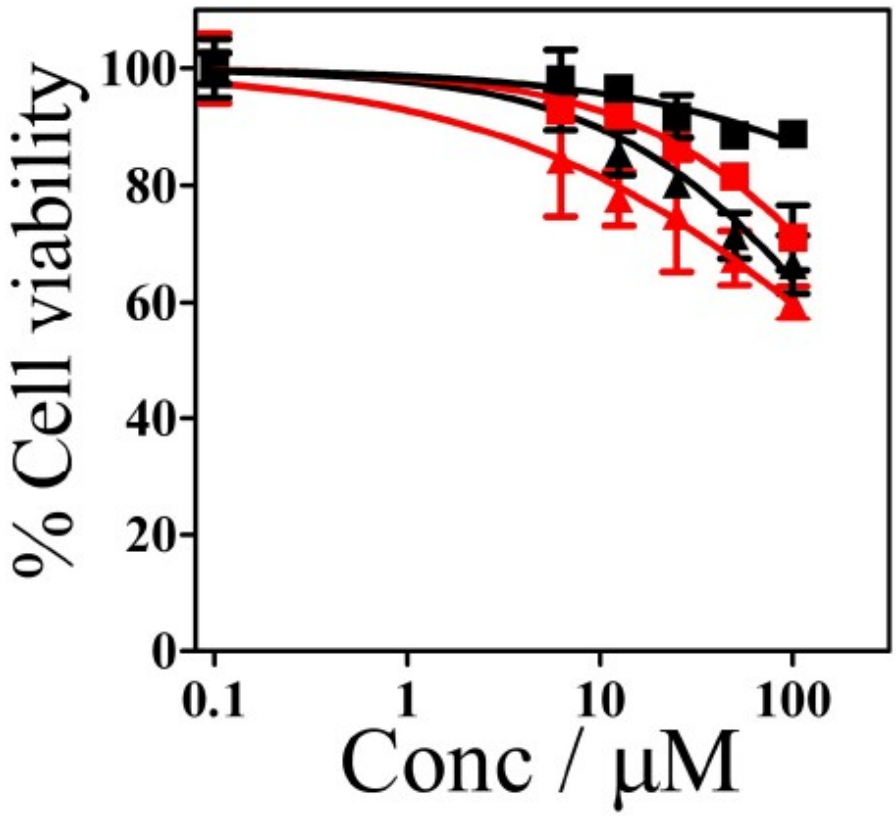

ESI Fig. S24. Photocytotoxicity of sal-lysH_2 (▲,▲) and $VOSO_4$ (■,■) in human cervical cancer HeLa cells on 2 h incubation in dark followed upon photo-irradiation to visible light (400 to 700 nm) as determined by MTT assay. The photo-exposed and dark-treated cells are shown by red (▲, ■) and black (▲, ■) symbols, respectively.

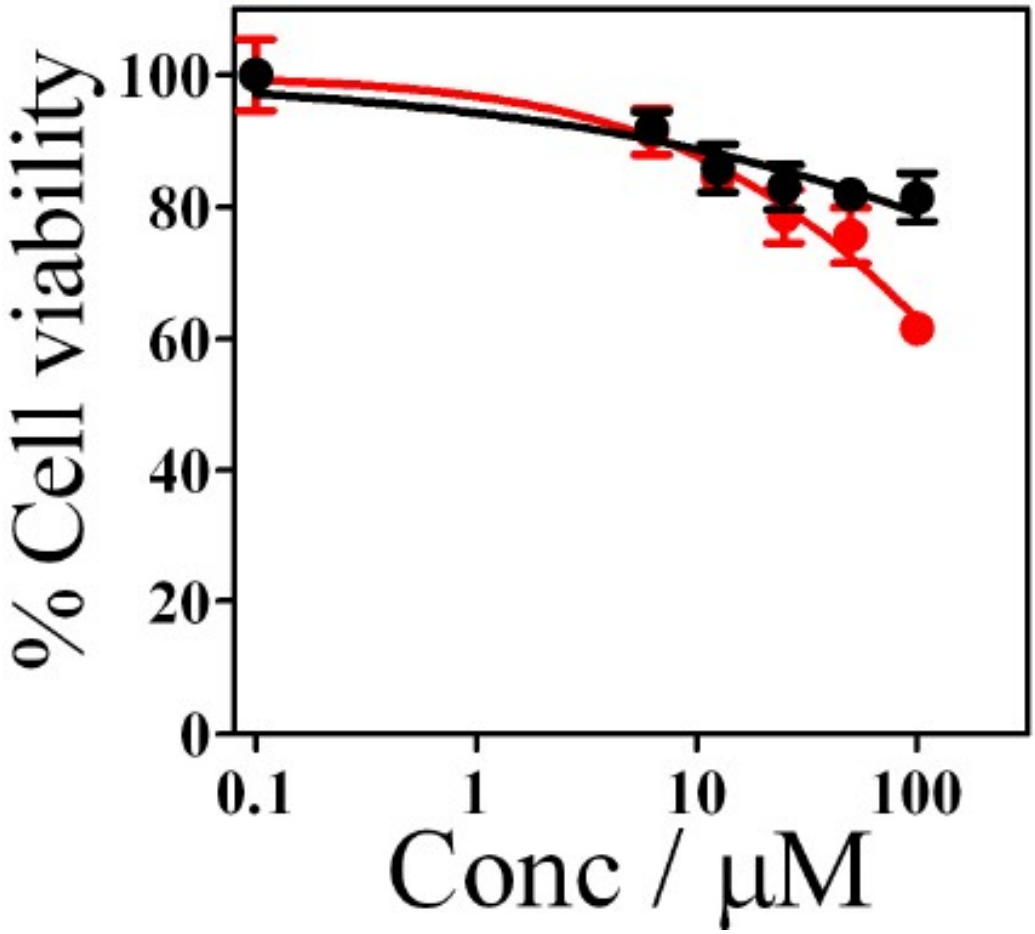

ESI Fig. S25. Photocytotoxicity of [VO(sal-argH)(phen)]Cl (**1**) in human cervical cancer HeLa cells on 2 h incubation in dark followed upon photo-irradiation to visible light (400 to 700 nm) as determined by MTT assay. The photo-exposed and dark-treated cells are shown by red (●) and black (●) symbols, respectively.

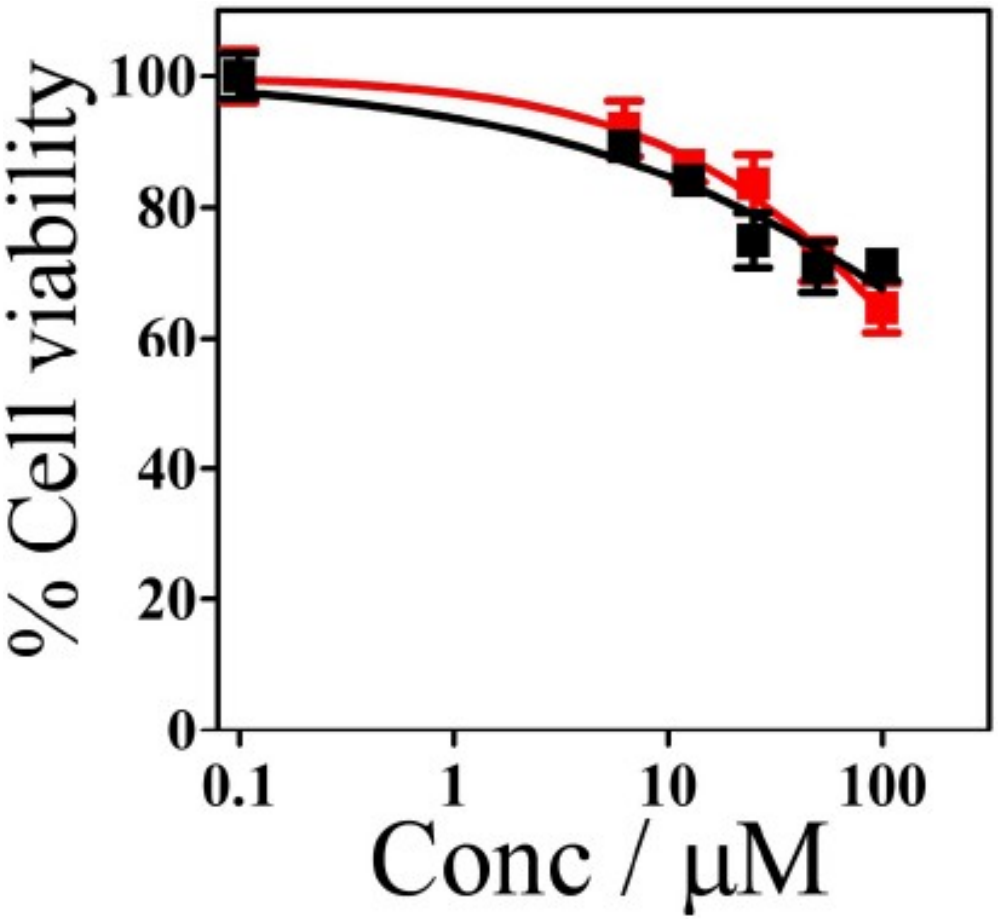

ESI Fig. S26. Photocytotoxicity of [VO(sal-argH)(dpq)]Cl (**2**) in human cervical cancer HeLa cells on 2 h incubation in dark followed upon photo-irradiation to visible light (400 to 700 nm) as determined by MTT assay. The photo-exposed and dark-treated cells are shown by red (■) and black (■) symbols, respectively.